HHS Public Access

Author manuscript

J Tissue Eng Regen Med. Author manuscript; available in PMC 2019 February 01.

Published in final edited form as:

J Tissue Eng Regen Med. 2018 February ; 12(2): 546–556. doi:10.1002/term.2568.

A Cardiac Patch from Aligned Microvessel and Cardiomyocyte Patches

Jeremy A. Schaefer[1], **Pilar A. Guzman**[3], **Sonja B. Riemenschneider**[2], **Timothy J. Kamp**[4], and **Robert T. Tranquillo**[1,2]

[1]Department of Biomedical Engineering, University of Minnesota, Minneapolis, MN

[2]Department of Chemical Engineering and Materials Science, University of Minnesota, Minneapolis, MN

[3]Department of Integrative Biology and Physiology, University of Minnesota, Minneapolis, MN

[4]Department of Medicine and Public Health, University of Wisconsin-Madison, Madison, WI

Abstract

Cardiac tissue engineering aims to produce replacement tissue patches in the lab to replace or treat infarcted myocardium. However, current patches lack pre-formed microvascularization and are therefore limited in thickness and force production. In the present study, we sought to assess whether a bi-layer patch composed of a layer made from human induced pluripotent stem cell-derived cardiomyocytes (hiPSC-CMs) and a microvessel layer composed of self-assembled human blood outgrowth endothelial cells (BOECs) and pericytes (PCs) was capable of engrafting on the epicardial surface of a nude rat infarct model and becoming perfused by the host four weeks after acute implantation. The bi-layer configuration was found to increase the twitch force production, improve hiPSC-CM survival and maturation, and increase patent microvessel lumens compared to time-matched single layer controls after two weeks of *in vitro* culture. Upon implantation, the patch microvessels sprouted into the CM layer of the patch and inosculated with the host vasculature as evidenced by species-specific perfusion labels and erythrocyte staining. Our results demonstrate the added microvessel layer of a bi-layer patch substantially improves *in vitro* functionality, and the bi-layer patch is capable of engraftment with rapid microvessel inosculation on injured myocardium. The bi-layer format will allow for scaling up in size through the addition of layers to obtain thicker tissues generating greater force in the future.

Keywords

tissue engineering; induced pluripotent stem cell-derived cardiomyocyte; engineered myocardium; engineered microvessel; cardiomyocyte; cardiomyocyte maturation

Corresponding author: Robert T. Tranquillo, Department of Biomedical Engineering, 7-114 NHH, 312 Church St SE, University of Minnesota, Minneapolis, MN 55455, Tel: 612-625-6868, Fax: 612-626-6583, tranquillo@umn.edu.

Disclosure of Potential Conflicts of Interest

T.J.K. is a compensated consultant for Cellular Dynamics International. The other authors indicated no potential conflicts of interest.

1. Introduction

Coronary heart disease accounts for nearly 1 in 7 deaths each year in the United States (Mozaffarian, *et al.*, 2016) with immediate death following myocardial infarction (MI) or progression to heart failure for many survivors. Current treatments are incapable of repairing cellular damage once it has occurred and are limited to preventing further damage and treating symptoms of the disease. The only available method to replace the failing myocardium is by orthotropic heart transplantation; however, this intervention is severely limited by the number of available donor hearts. This treatment deficiency has opened the door for cell- and engineered tissue-based therapies to recover heart function. Direct injections of cells into the infarcted myocardium have shown some success in the clinic. Bone marrow-derived stem cells (Suncion, *et al.*, 2014, Williams, *et al.*, 2011) and skeletal myoblasts (Herreros, *et al.*, 2003, Menasche, *et al.*, 2003, Smits, *et al.*, 2003) have been used in patients with some improvement in terms of wall thickness and ejection fraction. However, cell retention has been low (Terrovitis, *et al.*, 2009) and cardiac arrhythmias have been reported (Menasche, *et al.*, 2003). Cardiac patches constructed using tissue engineering principles may prove a reliable cell delivery vehicle for cells since they are associated with a scaffold to ensure their initial retention and survival via a cell niche. They also offer the potential for *in vitro* conditioning, such as mechanical loading (Mihic, *et al.*, 2014, Wendel, *et al.*, 2014) or electrical stimulation (Chan, *et al.*, 2013, Hirt, *et al.*, 2014), to improve cellular function and create a functional tissue prior to implantation.

The ultimate goal of cardiac tissue engineering is to fill the need for replacement donor tissues with tissues that can be grown in the lab. One of the main limitations is sourcing human cells, specifically cardiomyocytes, to use in generating tissues. With the discovery of induced pluripotent stem cells (iPSCs) (Yu, *et al.*, 2007) and the ability to efficiently differentiate functional cardiomyocytes (iPSC-CMs) (Lian, *et al.*, 2013) from them, this need may finally be met. hiPSC-CMs have been used to create patches by entrapment in matrices of primarily collagen (Tulloch, *et al.*, 2011) and fibrin (Hirt, *et al.*, 2014, Wendel, *et al.*, 2015) as well as cell sheets (Komae, *et al.*, 2015) and layer-by-layer (Amano, *et al.*, 2016) methods. A recent study has shown benefit from these tissues in reducing deleterious effects in a rodent model of myocardial infarction (Wendel, *et al.*, 2015).

Despite the advances made with cardiac patches, their size is severely limited by their lack of a pre-formed microvasculature to supply nutrients to the tissue. In order to grow tissues that are large enough to generate meaningful force in patients, a method to incorporate a vasculature *in vitro* is required. Previous studies from our group (Riemenschneider, *et al.*, 2016) and others (Chen, *et al.*, 2009, Chen, *et al.*, 2010, Mishra, *et al.*, 2016) have shown that engineered human microvessels can become rapidly inosculated and perfused by the host vasculature *in vivo*, including on the epicardial surface following infarction (Riemenschneider, *et al.*, 2016). These studies demonstrate the potential of a patch containing pre-formed microvessels being rapidly perfused once implanted in the host.

The present study reports the creation of bi-layer patch composed of a cardiomyocyte layer (CM) containing human iPSC-CMs and a microvessel layer (BPC) containing human blood outgrowth endothelial cells (BOECs) (Lin, *et al.*, 2000), a circulating endothelial cell type

isolated from blood with the potential of being autologously sourced, and human pericytes (PCs), a support cell type that stabilizes microvessels (Allt and Lawrenson, 2001). While there are other potentially autologous endothelial cell sources, such has iPSC-ECs (Taura, *et al.*, 2009), we maintained use of the BOECs for direct comparison to our prior studies (Riemenschneider, *et al.*, 2016). The two patches are formed separately by entrapping cells in a fibrin gel, and adhered together using fibrin 3–5 days later. The use of fibrin is advantageous because cardiac cells can readily degrade and remodel the fibrin matrix and replace it with a cell-produced extracellular matrix (Wendel, *et al.*, 2015, Wendel, *et al.*, 2014). The bi-layer and control patches were implanted in the same infarct model as our previous work (Riemenschneider, *et al.*, 2016, Wendel, *et al.*, 2015) after two weeks of static culture to determine the fate of the implanted microvessels. The ability of the microvessels to integrate with the CM layer of the bi-layer patch as well as the fraction of these microvessels that inosculated with the host vasculature was assessed. Due to the reduction in the total number of hiPSC-CMs implanted in the present study because of a methodological change compared to our previous work (Wendel, *et al.*, 2015), therapeutic effects were not expected, but were assessed with echocardiography and histological characterization of the scar.

2. Materials and Methods

2.1 Creation of aligned microvessel patches

Ridges were melted into the bottom of a 6 well tissue culture plate to form rectangular wells measuring 18.4×5 mm. A drop of sterile vacuum grease was applied at each end of the well using a sterile 3 ml syringe and a sterile porous polyethylene spacer (5×5 mm) was placed on top of the grease leaving a well measuring 8.4×5 mm. Droplets of fibrin gel forming solution containing BOECs and PCs (see Supplemental Information) were pipetted onto the inner edge of the spacers and dragged inward to fill the central well. Placing the droplets first is important to ensure the fibrin gel is integrated in the pores of the spacers, anchoring it in place and preventing longitudinal compaction. The fibrin forming solution was composed of 4 mg/ml fibrinogen (Sigma), 200 ng/ml stem cell factor (SCF), interleukin-3 (IL-3), and stromal derived factor 1α (SDF-1α), vascular endothelial growth factor (VEGF), basic fibroblast growth factor (bFGF) (R&D Systems), 1.82 M/ml BOECs, 0.36 M/ml PCs, 1.25 U/ml thrombin (Sigma), and Medium 199 basal medium (Gibco)(M199). The total volume of each gel was 120 μl. Samples were allowed to set in a sterile tissue culture hood for 10 minutes then transferred to a 37°C, 5% CO2 incubator for an additional 15 minutes before covering with 4 ml of BOEC medium + 2 mg/ml ε-aminocaproic acid (ACA) per well. Medium was changed at 24 hours and every other day thereafter.

After 5 days of culture, samples were detached from the bottom of the 6-well plate and carefully transferred to a new well. Spacers were anchored 8.4 mm apart on fresh drops of vacuum grease to maintain sample length. Detachment from the bottom of the well plate allows cell-induced lateral compaction which causes longitudinal alignment of microvessels and fibrin fibrils.

2.2 Creation of aligned hiPSC-CM patches

Culture wells were created identically to culture wells for aligned microvessel patches, and patches were formed in the same manner. Fibrin gel forming solution was composed of 4 mg/ml fibrinogen, 4 M/ml hiPSC-CMs (See Supplemental Information), 1.25 U/ml thrombin, and M199 basal medium. The total volume of each gel was 120 μl. Samples were allowed to set in a sterile tissue culture hood for 10 minutes then transferred to a 37°C, 5% CO2 incubator for an additional 15 minutes before covering with 4 ml of EB-20 + ACA medium per well. Medium was changed to EB-2 + ACA after 24 hours and changed every other day thereafter. hiPSC-CM patches were detached from the bottom of the 6-well plate in the same manner as microvessel patches; however, the hiPSC-CM gels were detached after 24 hours instead of 5 days due to the slower rate of cell-induced compaction of the hiPSC-CM gels.

2.3 Bi-layer patch formation

Microvessel and hiPSC-CM patches were cultured statically after detachment for 3–5 days before adhering them together (Figure 1). Medium was aspirated from both patches, and replaced with phosphate buffered saline (PBS) for 5 minutes to minimize residual serum left in constructs. Patches were then soaked in 10 mg/ml fibrinogen solution diluted in 20 mM HEPES in 37° C, 5% CO_2 incubator for 20 minutes. The fibrinogen solution was aspirated from the hiPSC-CM patch, and the microvessel patch was cut from its spacers. 10 μl of a 5 U/ml thrombin solution (with 2 mM $CaCl_2$ in DMEM+20 mM HEPES) was added to the surface of the hiPSC-CM patch, and the microvessel patch was carefully placed on top using sterile forceps. Bi-layer patches were allowed to set in the culture hood for 10 minutes, then in 37° C, 5% CO_2 incubator for 20 minutes before addition of EB-20 medium + ACA. Medium was changed to EB-2 hiPSC-CM maintenance medium (Zhang, *et al.*, 2009) + ACA 24 hours later and every other day thereafter. Bi-layer patches were cultured statically for 2 weeks before *in vitro* assessment or *in vivo* implantation. A subset of single-layer BPC and CM patches not used for bi-layer patch creation were cultured statically for 2 weeks to serve as time-matched controls.

2.4 Patch characterization

Two weeks after creating the bi-layer patches, a subset of bi-layer and single-layer BPC and CM control patches were fixed with 4% paraformaldehyde (PFA)(Electron Microscopy Sciences) for 1 hour at 4°C followed by rinses with PBS. Samples were cut in half and placed in infiltration solution 1 (30% w/V sucrose in PBS) at 4°C overnight and then transferred to infiltration solution 2 (50% infiltration solution 1, 50% embedding medium (TissueTek OCT)) for 4 hours at room temperature. Samples were frozen in embedding medium and 9 μm sections were cut for immunohistochemical staining. Sections were permeabilized with 0.1% Triton-X100 for 10 minutes, rinsed with PBS three times for 5 minutes each, blocked in 5% normal donkey serum (Jackson Immunoresearch) for 2 hours, and incubated in primary antibodies against specific antigens at 4°C overnight in blocking solution. Sections were rinsed with three 5 minute incubations of PBS before adding secondary antibodies for 1 hour in a solution of Hoechst 33342 diluted 1:10,000 at room temperature. See Supplemental Table 1 for antibody dilutions.

2.5 Experimental design

Four groups were evaluated in this study: 1. MI + bi-layer patch CM side down onto infarct (CM down) (N=7), 2. MI + bi-layer patch microvessel side down onto infarct (BPC down) (N=7), 3. MI + CM patch only (CM-only) (N=6), and 4. MI + empty suture knots in the epicardial surface (sham) (N=8). Both orientations of the bi-layer patch were tested to ascertain any orientation dependence. The CM-only group served as an avascular control. The sham group served as patch free control, while still having the puncture wound and the absorbable sutures used to attach the tissue patches (to control for any effect of the suture degradation products). Other control groups (e.g. double-layered CM and BPC patches) were considered less informative or previously examined (i.e. fibrin-only patches (Wendel, *et al.*, 2014) and excluded to make the design feasible.

2.6 Implantation of patches into an acute nude rat infarct model

Procedures used in this study were reviewed and approved by the Institutional Animal Care and Use Committee and Research Animal Resources at the University of Minnesota and conform to NIH guidelines for care and use of laboratory animals.

Twenty-eight female Foxn1rnu nude rats (Envigo) were used in this study, aged 8–9 weeks old and weighing 150–200 g. Isoflurane was administered for anesthesia, and rats were intubated and ventilated for the duration of surgery. The chest was open via sternotomy to expose the heart, and the LAD was permanently ligated to achieve the MI, evident by color change on the epicardial surface. Once established, two patches were cut from the porous spacers and sutured parallel to one another over the infarcted region for treatment groups. For the sham group, four knots were placed in the epicardium in the approximate location of patch sutures to replicate the puncture wound and suture degradation to which the treatment groups were exposed. After patch placement, the chest was closed and the animals were allowed to recover.

2.7 Cardiac functional measurements

Echocardiography (Vevo 2100 system) was conducted prior to implantation and at two follow-up time points: 1 week and 4 weeks post implantation. Ejection fraction and fractional shortening were determined from two long axis and three short axis views from each animal at each time point.

2.8 *In vivo* vessel perfusion

After the week four echocardiogram, animals were anesthetized with isoflurane and the chest was reopened. Immediately prior to sacrifice, human and rat specific endothelial labels, rhodamine-conjugated ulex europaeus agglutinin – I (UEA-I) (Vector Laboratories) and fluorescein-conjugated griffonia simplicifolia lectin I, isolectin B4 (IB4)(Vector Laboratories), respectively, were injected into the left ventricle and allowed to circulate for 1 minute. Circulating for longer time becomes ineffective as the animal’s heart begins to slow without ventilation. The animal was then euthanized with an intracardiac injection of potassium chloride prior to explanting the heart.

2.9 Infarct assessment

Masson's trichrome stain was used to characterize the infarct size and scar wall thickness. The infarct size was measured in terms of the percent area of the LV free wall occupied by scar. Values for a single animal were determined from transverse sections of the heart. Scar thickness was determined by averaging 9–12 measurements of LV thickness in the region occupied by scar.

2.10 Perfusion analysis

Cryosections were fluorescently stained and imaged to visualize all human vessels, as well as perfused human and rat vessels at the time of explantation. Perfused rat vessels were labeled with fluorescein (488 nm excitation) via IB4, perfused human vessels labeled with rhodamine (561 nm excitation) via UEA-1, and all human vessels labeled with Cy5 (647 nm excitation) via hCD31 (Dako) to allow separation of vessel types. The fraction of perfused human vessels was determined by comparing the number of hCD31+ vessels that were co-labeled by the perfusion labels with those that were only hCD31+. Because PCs express GFP, rat perfused vessels and PCs were distinguished by morphology. A green lumen structure was considered a recruited pericyte if the interior of the lumen contained positive stain for hCD31. All other green lumen-like structures were considered perfused rat vessels.

2.11 Cardiomyocyte and vessel alignment characterization

Heart sections were stained for f-actin using rhodamine conjugated phalloidin (Invitrogen) counterstained with hCD31 to detect human microvessels. Cardiomyocyte orientation in the CM layer of the bi-layer patch or CM only patch was analyzed from the f-actin stain using the Measure feature of the OrientationJ plugin (Fonck, *et al.*, 2009, Rezakhaniha, *et al.*, 2012) for ImageJ. The entire patch was imaged and assembled into a stitched image. Small subsections of the patch were analyzed at a time due to the curvature of the patch on the epicardial surface. Then, the angles of the human and rat vessels were measured in each subsection and compared to the average angle of the cardiomyocytes of that section.

2.12 Statistical analysis

Data are represented as mean ± standard deviation. Student's t-tests were performed in Excel. Multiple groups were compared with 1-way analysis of variance (ANOVA) with Tukey's HSD post-hoc tests in Minitab or IBM SPSS. P-values < 0.05 were considered significant.

3. Results

3.1 *In vitro* characterization

Both the CM-only and BPC-only patches became aligned via cell-induced vertical compaction from time of casting and lateral compaction after the gels were detached from the bottom surface of the culture plate. Final patch dimensions are listed in Supplemental Table 2. Longitudinal sectioning of the bi-layer patch at the end of the additional two weeks of culture following adherence of CM-only and BPC-only patches together revealed that alignment was maintained in both the CM and BPC layers (Figure 2B). The final CM

density was measured from cross-sectional views of the patches. After two weeks, the density was significantly greater in the CM layer of the bi-layer patch compared to a time-matched CM-only patch (237.0 ± 10.7 vs. 35.2 ± 9.4 CM/mm^2, N=4, $p<0.05$) (Figure 2C–D). Assuming that cells were evenly distributed throughout the construct at the time of casting, and limited cell migration, the approximate total CM count was estimated based on the number of cells in a cross sectional slice. This results in count estimates of 497k ± 35k vs 146k ± 44k for the bi-layer patch and CM-only patch, respectively. Staining for the apoptosis marker annexin V revealed that CM-only samples had more cTnT+ cells undergoing apoptosis than the bi-layer samples (75.4 ± 15.3% (N=3) vs. 37.5 ± 15.5% (N=5), respectively, $p<0.05$).

Cross-sections were also used to investigate the health of the microvessels two weeks after forming the bi-layer patches. The bi-layer patches maintained lumens in the BPC layer (Figure 2A). Final lumen density was compared between the BPC layer of the bi-layer patch and time-matched single layer BPC patches. The bi-layer patches contained more lumens than the BPC-only control (34 ± 12 vs 7 ± 3 lumens/mm^2, N=4, $p<0.05$).

Both CM-only patches and bi-layer patches (Supplemental Online Video 1 and Supplemental Online Video 2, respectively) beat spontaneously and produced measureable twitch forces when paced with field stimulation. The force of the bi-layer patch increased between one and two weeks, whereas the CM-only patches did not show improvement with time. At both one week and two weeks post adhering, the bi-layer patches produced more force than the CM-only controls. These differences were true when comparing both the force and the force normalized to the number of input CMs at the time of sample casting (Figure 3, $p<0.05$). The force per input CM has been proposed as a measure of the of “patch efficiency” (Zhang, *et al.*, 2013) as it attempts to incorporate how the final functional output is affected by the input conditions.

Western blot analysis (see Supplemental Information) of the CM-only and CM layer of the bi-layer patch was conducted to determine potential differences in CM maturation during *in vitro* culture. The primary focus was to compare the ratio of the mature isoform cTnI to the immature isoform ssTnI, as proposed previously (Bedada, *et al.*, 2014). This has been suggested as better maturation marker as the conversion from ssTnI to cTnI is complete, with the adult CMs containing only cTnI (Bhavsar, *et al.*, 1991, Sasse, *et al.*, 1993). This conversion is non-reversible in stress or disease conditions (Cumming, *et al.*, 1995, Sasse, *et al.*, 1993), unlike other common maturation markers. SERCA2A, a calcium pump on the sarcoplasmic reticulum, was also investigated. It was found that the cTnI:ssTnI ratio was approximately 3-fold higher in the bi-layer patch than in CM-only patch; however, there was no difference in SERCA2A expression (Supplemental Figure 1).

3.2 Patch engraftment

The patches characterized above (Figure 4A) were implanted acutely onto infarcted rat hearts (Figure 4B). Four weeks after implantation, the epicardial surface was covered with a thin, white layer of tissue covering most of the LV surface. After assessment, this layer was found to be patch surrounded by scar tissue (Figure 5A). The patch was found in all study animals after explantation resulting in an engraftment rate of 100%. The patch was found to

be composed of CMs packed too densely to identify individual cells. We verified these cells were hiPSC-CM through staining for human nuclear antigen (Supplemental Figure 2). At high magnification, sarcomeric banding could be easily seen in these CMs (Figure 5C). The patches ranged from 200–250 μm thick on the epicardial surface, but there were no differences in thickness between groups (Figure 5B). While the CM layer of the bi-layer patch and the CM-only patch were found in all animals, the BPC layer of the bi-layer patch was rarely found after four weeks *in vivo* due to apparent resorption of the layer as the human microvessels invaded the CM layer. Staining for f-actin and examination of orientation revealed the CMs were aligned circumferentially around the heart (Figure 5D). This is consistent with the orientation of the aligned patches upon implantation (Figure 4B).

3.3 *In vivo* vessel characterization and perfusion assessment

The total number of human microvessels as well as the number of perfused human and rat vessels that sprouted into the CM layer of the bi-layer patch and into the CM-only patch were quantified (Figure 6). Staining with human-specific CD31 (hCD31) antibody revealed no difference in the total number of human vessels between the two orientations of the bi-layer patch (65 ± 55.1 vs 48 ± 52 vessels/mm^2, CM down and BPC down, respectively). The percent of perfused human vessels was determined by comparing the co-localization of the UEA-I label injected prior to sacrifice and hCD31. Perfusion was verified by immunofluorescence stain for rat RBCs (Supplemental Figure 3A). One animal that died at two weeks post-implantation contained human microvessels throughout the thickness of the CM layer that were filled with blood (Supplemental Figure 3B). There was no difference in the perfused fraction of the human vessels in either orientation of the bi-layer patch (67 ± 28% vs 53 ± 33%, CM down and BPC down, respectively). Perfused rat vessels in the CM layer of the bi-layer patches or CM-only patch were quantified using the perfusion label IB4. Similarly, there was no difference between any of the groups (104 ± 52, 44 ±23, 96 ±61 vessels/mm^2 for CM-only, CM down, and BPC down respectively). The total number of vessels, human and perfused rat, was not different between groups either (104 ± 52, 108 ± 70, 144 ± 66 vessels/mm^2; CM-only, CM down, BPC down, respectively).

The alignment of rat and human vessels (Figure 5D) of a subset of animals (N=4) was measured relative to the local CM alignment determined with f-actin staining. The difference in mean angle alignment was 5.8 ± 40.2° for human vessels and 12.1 ± 39.0° for rat vessels indicating strong co-alignment of the microvessels growing into the aligned CM layer.

3.4 Left ventricle remodeling

The extent of LV remodeling was determined using Masson's trichrome staining. The size of the scar four weeks after surgery as a function of LV free wall area occupied by scar, and the thickness of the scar are summarized in Figure 7. The patch was excluded from these measurements when identified (e.g. Figure 5A), and no scar tissue on the outside of the patch was included in the thickness measurement. No difference was observed in the percent area of the scar between any of the implant groups and sham group (30.6 ± 6.2%, 37.6 ± 10.3%, 36.2 ± 5.4%, 37.4 ± 7.7% for CM down, BPC down, CM-only, and sham, respectively). However, the scar thickness in the bi-layer patch groups (CM down and BPC down) were thicker than the sham group (1443 ± 511 μm and 1403 ± 360 μm vs 862 ± 84

μm, respectively, $p<0.05$), whereas the CM-only group was not different than sham (1200 ± 363 μm vs 862 ± 84 μm, respectively).

3.5 Cardiac functional changes

Cardiac function was assessed using echocardiography. Long- and short-axis echocardiograms were collected prior to infarction and post-infarction at 1 and 4 weeks. Ejection fraction and fractional shortening were calculated at each time point (Supplemental Figure 4). No difference was found in either measurement between any of the groups and sham.

4. Discussion

This study demonstrated that adhering a hiPSC-CM patch and a human microvessel patch together with fibrin results in a human bi-layer cardiac patch that, after two weeks *in vitro*, produces substantially greater twitch force, greater CM survival, and enhanced CM maturation compared to a CM-only control patch. After four weeks *in vivo*, the microvessels from the BPC layer of the patch were able to sprout into the CM portion of the patch, become inosculated with the host vasculature, and perfused with blood. Our previous studies have demonstrated the beneficial effect of CM patches acutely placed on the epicardial surface of an infarcted rat heart (Wendel, *et al.*, 2015, Wendel, *et al.*, 2014). We have also previously shown in the same model that microvessel patches implanted on infarcted epicardium become inosculated with the host vasculature after 6 days and perfused with blood (Riemenschneider, *et al.*, 2016). The present study focused on combining a CM patch with a microvessel patch that could rapidly be perfused *in vivo*.

The bi-layer patch format provided substantial benefit to both layers of the patch as summarized above. The mechanism behind this benefit is uncertain; however, the functional outcomes are clear. Both bi-layer and CM-only patches exhibited measurable twitch forces. The CM-only patches (0.3 nN/input CM) of the present study, which were made directly from the differentiated hiPSCs, were similar to our previously reported hiPSC-CM+PC patches (0.2 nN/input CM)(Wendel, *et al.*, 2015), where we purified the differentiated hiPSCs for CMs and replaced the non-CM fraction with hPCs. The bi-layer patches (2.17 nN/input CM) were an improvement over our previously reported patches made from neonatal rat heart isolates (1.2 nN/input CM) (Wendel, *et al.*, 2014), although less contractile than patches made from hESC-CMs (5.7 nN/input CM) (Zhang, *et al.*, 2013). The reason for the nearly 10-fold increased twitch force observed in the bi-layer patch compared to the CM-only patch appears to have two causes. First, the number of CMs at the time of force testing was greater in the bi-layer patches. Staining for annexin V revealed that the difference in cell number is due largely to increased apoptosis of cTnT+ cells in the CM-only patch after two weeks of *in vitro* culture. It has been shown that endothelial cells protect CMs from apoptosis, potentially through neuroregulins (Zhao, *et al.*, 1998) or PDGF (Hsieh, *et al.*, 2006) pathways. While the difference in cell number certainly contributed to the difference in twitch force, the twitch force produced by the bi-layer patch was nearly 7.5x that of the CM-only patch, while the final bi-layer patch CM count was only 3.4x that of the CM-only patch. The second factor is apparent increased maturation of the CMs in the bi-layer patch. It

has been shown in mice that the force produced by cardiomyocytes increases with age from the embryonic to adult phenotype (Siedner, *et al.*, 2003). The 3-fold increased ratio of cTnI:ssTnI in the bi-layer patch CMs indicates a switch to a more mature phenotype in the present study. As the replacement of ssTnI with cTnI is irreversible and complete in the adult CM (Bhavsar, *et al.*, 1991, Sasse, *et al.*, 1993, Siedner, *et al.*, 2003), the bi-layer patch format confers CM maturation that is absent in the CM-only patch. The increased compaction in the CM layer of the bi-layer patch is not surprising due to the increased cellularity of the patch. While it is possible this increased compaction and associated increased CM density influences force production, it is difficult to determine to what extent due to the differences in cellularity and CM maturity between bi-layer and CM-only patches. The benefit to the BPC layer of the bi-layer patch is the increase in observed microvessel lumens. This could be due to reduced compaction of the BPC layer of the bi-layer patch because it was “fixed” on the bottom surface to the CM layer. A diffusible factor released from the CM layer that inhibits cell-induced compaction by the PCs or BOECs may also have reduced compaction of the BPC layer. We have previously shown excessive compaction of the fibrin gel can lead to collapse of microvessel lumens (Morin, *et al.*, 2014).

After two weeks of *in vitro* culture, the two layers of the bi-layer patch were well integrated. Initially, the interface between the two layers is relatively fragile until cells remodel the fibrin and stabilize it. The fragile nature of the boundary limited examination of the potential benefits of mechanical conditioning of the bi-layer patches that has been shown beneficial by us (Wendel, *et al.*, 2014) and others (Nunes, *et al.*, 2013). With time, we found that some of the supporting PCs were able to migrate across the interface between the two layers, but no microvessels migrated into the CM layer prior to implantation. However, we did find extensive microvessel sprouting into the CM layer of the patch after four weeks *in vivo*. More importantly, a large portion of the human microvessels had inosculated with the host vasculature and become perfused. Previously, we have shown that this inosculation occurs within the implanted patch near the interface when host vasculature migrates into the patch (Riemenschneider, *et al.*, 2016). This is a promising result for future studies with thicker patches that can generate physiologically-relevant force as it will be imperative to establish perfusion of the patch quickly to prevent necrosis. As evidenced by one animal that died two weeks after implantation, microvessel sprouting throughout the full thickness of the CM layer, including perfusion of the vessels with blood (Supplemental Figure 3B), can occur in as little as two weeks. Although inosculation happens quickly and host vasculature and support cells may facilitate long term stabilization of the human microvessels *in vivo*, PCs are still required in our patch to stabilize the microvessels over the three weeks of *in vitro* culture. The microvascular remodeling of the patch that occurred *in vivo* was most likely caused by the drastically different microenvironment in the hypoxic and nutrient-deficient infarct region. The bi-layer patches were relatively thin, and adequately supplied with nutrients and oxygen *in vitro* solely by diffusion from the surrounding culture medium, as no necrotic regions were observed. Once implanted, the CMs likely experienced stress from the lack of a nutrient rich medium bath and released angiogenic factors, potentially through exosomes (Garcia, *et al.*, 2015). It has also been shown that global expression of vascular endothelial growth factor (VEGF), a potent angiogenic factor, is increased in the myocardium following ischemia (Banai, *et al.*, 1994).

The thickness of the CM-only and of the bi-layer patch in both orientations was the same at explantation. This result is surprising considering the difference in thickness and in cellularity between the bi-layer and CM-only patches at the time of implantation. However, cell behavior *in vitro* is not always indicative of cell behavior *in vivo.* The combination of three factors *in vivo* could have led to this observation. First, greater cell death in the bi-layer patch after implantation would reduce the difference in cellularity between bi-layer and CM-only patches. Second, greater proliferation of CMs in the CM-only patch would also have the same effect. It has been shown previously that adult rat CMs do not engraft in healthy or damaged myocardium whereas fetal and neonatal cells do (Reinecke, *et al.*, 1999). While the cells used in the present study are not adult, the difference in maturation state of the bi-layer CMs and CM-only patch CMs could lead to differences in cell survival *in vivo.* Third, hypertrophy of the CMs in the CM-only patches would result in larger cells occupying more space per cell than their bi-layer patch counterparts. Because all three of these factors potentially play a role in the observation of similar patch thickness at explantation, it is difficult to discriminate which factor, if any, is dominant. This observation does not, however, negate the benefit of developing a bi-layer tissue as a precursor towards generating a thick, microvascularized cardiac tissue.

Both human and rat microvessels that migrated into the CM layer and CM-only patch were found to co-align with the implanted CMs. This co-alignment was likely caused by cell contact guidance, where cells preferentially migrate bidirectionally in response to aligned extracellular matrix fibrils (Dickinson, *et al.*, 1994). This has been demonstrated with endothelial cells in collagen-nanofiber hydrogels (Laco, *et al.*, 2013) and fibrin hydrogels (Morin and Tranquillo, 2011). In the present study, the patch was primarily aligned fibrin at the time of implantation. The sprouting endothelial cells may have followed these fibrin fibrils as they migrated into the CM layer of the patch. Cell-produced ECM post-implantation or the aligned CMs may also have provided contact guidance cues for the migrating endothelial cells.

The cardiac functional results from this study did not match the benefit seen in our previous work (Wendel, *et al.*, 2015, Wendel, *et al.*, 2014). However, the procedure for adhering the microvessel layer to the CM layer necessitated changing how the CM layer was formed. Previously, a tubular mold was used to make an aligned ring construct which was cut into three patches that were sutured onto the epicardium (Wendel, *et al.*, 2015, Wendel, *et al.*, 2014). The slab format used in the present study yielded patches with much smaller total initial volume (240 μl vs. 1.25 ml). Despite the increased cardiomyocyte seeding density (4 M/ml vs. 2 M/ml) utilized in the present study, which was determined during initial optimization experiments in the new system, the change in patch formation strategy resulted in fewer than half of the total number of CMs delivered to the epicardium compared to our previous study. This reduction in cell content would greatly reduce the amount of any paracrine signals released from the patch that could have a beneficial effect on the surrounding myocardium, as neither mechanical support nor electrical coupling and contractile support were implicated in the functional beneficial effect seen previously due to the thin layer of scar that forms between the epicardial surface and the patch, precluding electromechanical coupling (Wendel, *et al.*, 2015). In both these studies, although the CM density in the patch increased considerably during implantation from the pre-implant value

of 200–400 CM/mm^2, the final density was likely lower than that for adult human myocardium. Despite a lower CM density and the electromechanical isolation of the patch from the thin scar layer, the putative paracrine factor benefit can be sufficient to nearly eliminate the effects of infarction in this model (Wendel, *et al.*, 2014). However, development of strategies to obviate the thin scar layer are of obvious interest for epicardial patch placement.

Future studies could be directed at trying to simulate the infarcted environment *in vitro* to induce vessel formation into the CM layer. One way to accomplish this might be through the use of a hypoxic incubator. The reduced oxygen would simulate the stress that the CMs experience in the infarct region from reduced blood flow. A method to induce local hypoxia in the CM patch could be to increase the metabolic activity of the CMs by introducing a drug that increases contraction rate, such as isoproterenol, or through the use of electrical stimulation during *in vitro* culture. Electrical stimulation also has been shown to improve functional outcomes of CMs including increased force production (Hirt, *et al.*, 2014) and CM maturation (Chan, *et al.*, 2013).

While the approach detailed here yields an engineered cardiac tissue in close proximity to a microvessel network, the final patch thickness remains too small for use beyond a rodent model. In the future, multiple bi-layer patches could be adhered together using the same method to create a thicker patch that generates physiologically relevant force. By creating a thicker tissue, one could also better simulate *in vitro* the stressed environment the CMs experience *in vivo*, which could lead to microvessels sprouting into the CM layers prior to implantation. Attaching the microvessel patch to an external perfusion pump, preferably through a larger diameter vessel integrated into the microvessel patch, could also help induce sprouting into the CM patch. Previous studies have shown the benefit of flow for improving microvessel network properties (Hernandez Vera, *et al.*, 2009, Morin, *et al.*, 2014).

5. Conclusions

We created a bi-layer cardiac patch made from an hiPSC-CM layer and a self-assembled human microvessel layer. After two weeks of culture, this arrangement led to increased force production, improved CM survival and maturation, and increased microvessel density when compared to time-matched single-layer controls. These results demonstrate the dramatic effect microvascular networks can have on hiPSC-CMs as a living and complementary component of engineered cardiac tissues. Upon implantation into a nude rat acute myocardial infarction model for four weeks, the bi-layer patches reduced LV wall thinning compared to sham animals. The CM layer of the bi-layer patches became dense and was invaded by human and rat microvessels that were co-aligned with the CMs and perfused by the host. We believe this study demonstrates a potential method to produce thicker, more contractile patches in the future by increasing the number of layers adhered together.

Supplementary Material

Refer to Web version on PubMed Central for supplementary material.

Acknowledgments

This work was supported by NIH Grant R01 HL108670 (to R.T.T). We thank Susan Saunders, Jackson Baril, and Jake Siebert for their technical assistance.

Research supported by the National Institutes of Health grant R01 HL108670 (to RTT)

References

Allt G, Lawrenson JG. Pericytes: cell biology and pathology. Cells Tissues Organs. 2001; 169(1):1–11. [PubMed: 11340256]

Amano Y, Nishiguchi A, Matsusaki M, et al. Development of vascularized iPSC derived 3D-cardiomyocyte tissues by filtration Layer-by-Layer technique and their application for pharmaceutical assays. Acta Biomater. 2016; 33:110–121. [PubMed: 26821339]

Banai S, Shweiki D, Pinson A, et al. Upregulation of vascular endothelial growth factor expression induced by myocardial ischaemia: implications for coronary angiogenesis. Cardiovasc Res. 1994; 28(8):1176–1179. [PubMed: 7525061]

Bedada FB, Chan SS, Metzger SK, et al. Acquisition of a quantitative, stoichiometrically conserved ratiometric marker of maturation status in stem cell-derived cardiac myocytes. Stem Cell Reports. 2014; 3(4):594–605. [PubMed: 25358788]

Bhavsar PK, Dhoot GK, Cumming DV, et al. Developmental expression of troponin I isoforms in fetal human heart. FEBS Lett. 1991; 292(1–2):5–8. [PubMed: 1959627]

Chan YC, Ting S, Lee YK, et al. Electrical stimulation promotes maturation of cardiomyocytes derived from human embryonic stem cells. J Cardiovasc Transl Res. 2013; 6(6):989–999. [PubMed: 24081385]

Chen X, Aledia AS, Ghajar CM, et al. Prevascularization of a fibrin-based tissue construct accelerates the formation of functional anastomosis with host vasculature. Tissue Eng Part A. 2009; 15(6): 1363–1371. [PubMed: 18976155]

Chen X, Aledia AS, Popson SA, et al. Rapid anastomosis of endothelial progenitor cell-derived vessels with host vasculature is promoted by a high density of cotransplanted fibroblasts. Tissue Eng Part A. 2010; 16(2):585–594. [PubMed: 19737050]

Cumming DV, Seymour AM, Rix LK, et al. Troponin I and T protein expression in experimental cardiac hypertrophy. Cardioscience. 1995; 6(1):65–70. [PubMed: 7605898]

Dickinson RB, Guido S, Tranquillo RT. Biased cell migration of fibroblasts exhibiting contact guidance in oriented collagen gels. Ann Biomed Eng. 1994; 22(4):342–356. [PubMed: 7998680]

Fonck E, Feigl GG, Fasel J, et al. Effect of aging on elastin functionality in human cerebral arteries. Stroke. 2009; 40(7):2552–2556. [PubMed: 19478233]

Garcia NA, Ontoria-Oviedo I, Gonzalez-King H, et al. Glucose Starvation in Cardiomyocytes Enhances Exosome Secretion and Promotes Angiogenesis in Endothelial Cells. PLoS One. 2015; 109:e0138849. [PubMed: 26393803]

Hernandez Vera R, Genove E, Alvarez L, et al. Interstitial fluid flow intensity modulates endothelial sprouting in restricted Src-activated cell clusters during capillary morphogenesis. Tissue Eng Part A. 2009; 15(1):175–185. [PubMed: 18636940]

Herreros J, Prosper F, Perez A, et al. Autologous intramyocardial injection of cultured skeletal muscle-derived stem cells in patients with non-acute myocardial infarction. Eur Heart J. 2003; 24(22): 2012–2020. [PubMed: 14613737]

Hirt MN, Boeddinghaus J, Mitchell A, et al. Functional improvement and maturation of rat and human engineered heart tissue by chronic electrical stimulation. Journal of Molecular and Cellular Cardiology. 2014; 74:151–161. [PubMed: 24852842]

Hsieh PC, Davis ME, Gannon J, et al. Controlled delivery of PDGF-BB for myocardial protection using injectable self-assembling peptide nanofibers. The Journal of Clinical Investigation. 2006; 116(1):237–248. [PubMed: 16357943]

Komae H, Sekine H, Dobashi I, et al. Three-dimensional functional human myocardial tissues fabricated from induced pluripotent stem cells. Journal of Tissue Engineering and Regenerative Medicine. 2015

Laco F, Grant MH, Black RA. Collagen-nanofiber hydrogel composites promote contact guidance of human lymphatic microvascular endothelial cells and directed capillary tube formation. J Biomed Mater Res A. 2013; 101(6):1787–1799. [PubMed: 23197422]

Lian X, Zhang J, Azarin SM, et al. Directed cardiomyocyte differentiation from human pluripotent stem cells by modulating Wnt/beta-catenin signaling under fully defined conditions. Nat Protoc. 2013; 8(1):162–175. [PubMed: 23257984]

Lin Y, Weisdorf DJ, Solovey A, et al. Origins of circulating endothelial cells and endothelial outgrowth from blood. The Journal of Clinical Investigation. 2000; 105(1):71–77. [PubMed: 10619863]

Menasche P, Hagege AA, Vilquin JT, et al. Autologous skeletal myoblast transplantation for severe postinfarction left ventricular dysfunction. Journal of the American College of Cardiology. 2003; 41(7):1078–1083. [PubMed: 12679204]

Mihic A, Li J, Miyagi Y, et al. The effect of cyclic stretch on maturation and 3D tissue formation of human embryonic stem cell-derived cardiomyocytes. Biomaterials. 2014; 35(9):2798–2808. [PubMed: 24424206]

Mishra R, Roux BM, Posukonis M, et al. Effect of prevascularization on in vivo vascularization of poly(propylene fumarate)/fibrin scaffolds. Biomaterials. 2016; 77:255–266. [PubMed: 26606451]

Morin KT, Dries-Devlin JL, Tranquillo RT. Engineered microvessels with strong alignment and high lumen density via cell-induced fibrin gel compaction and interstitial flow. Tissue Eng Part A. 2014; 20(3–4):553–565. [PubMed: 24083839]

Morin KT, Tranquillo RT. Guided sprouting from endothelial spheroids in fibrin gels aligned by magnetic fields and cell-induced gel compaction. Biomaterials. 2011; 32(26):6111–6118. [PubMed: 21636127]

Mozaffarian D, Benjamin EJ, Go AS, et al. Heart Disease and Stroke Statistics-2016 Update: A Report From the American Heart Association. Circulation. 2016; 133(4):e38–e360. [PubMed: 26673558]

Nunes SS, Miklas JW, Liu J, et al. Biowire: a platform for maturation of human pluripotent stem cell-derived cardiomyocytes. Nat Methods. 2013; 10(8):781–787. [PubMed: 23793239]

Reinecke H, Zhang M, Bartosek T, et al. Survival, integration, and differentiation of cardiomyocyte grafts: a study in normal and injured rat hearts. Circulation. 1999; 100(2):193–202. [PubMed: 10402450]

Rezakhaniha R, Agianniotis A, Schrauwen JT, et al. Experimental investigation of collagen waviness and orientation in the arterial adventitia using confocal laser scanning microscopy. Biomech Model Mechanobiol. 2012; 11(3–4):461–473. [PubMed: 21744269]

Riemenschneider SB, Mattia DJ, Wendel JS, et al. Inosculation and perfusion of pre-vascularized tissue patches containing aligned human microvessels after myocardial infarction. Biomaterials. 2016; 97:51–61. [PubMed: 27162074]

Sasse S, Brand NJ, Kyprianou P, et al. Troponin I gene expression during human cardiac development and in end-stage heart failure. Circulation Research. 1993; 72(5):932–938. [PubMed: 8477526]

Siedner S, Kruger M, Schroeter M, et al. Developmental changes in contractility and sarcomeric proteins from the early embryonic to the adult stage in the mouse heart. J Physiol. 2003; 548(Pt 2): 493–505. [PubMed: 12640016]

Smits PC, van Geuns RJ, Poldermans D, et al. Catheter-based intramyocardial injection of autologous skeletal myoblasts as a primary treatment of ischemic heart failure: clinical experience with six-month follow-up. Journal of the American College of Cardiology. 2003; 42(12):2063–2069. [PubMed: 14680727]

Suncion VY, Ghersin E, Fishman JE, et al. Does transendocardial injection of mesenchymal stem cells improve myocardial function locally or globally?: An analysis from the Percutaneous Stem Cell Injection Delivery Effects on Neomyogenesis (POSEIDON) randomized trial. Circulation Research. 2014; 114(8):1292–1301. [PubMed: 24449819]

Taura D, Sone M, Homma K, et al. Induction and isolation of vascular cells from human induced pluripotent stem cells–brief report. Arterioscler Thromb Vasc Biol. 2009; 29(7):1100–1103. [PubMed: 19423866]

Terrovitis J, Lautamaki R, Bonios M, et al. Noninvasive quantification and optimization of acute cell retention by in vivo positron emission tomography after intramyocardial cardiac-derived stem cell delivery. Journal of the American College of Cardiology. 2009; 54(17):1619–1626. [PubMed: 19833262]

Tulloch NL, Muskheli V, Razumova MV, et al. Growth of Engineered Human Myocardium With Mechanical Loading and Vascular Coculture. Circulation Research. 2011; 109(1):47–59. [PubMed: 21597009]

Wendel JS, Ye L, Tao R, et al. Functional Effects of a Tissue-Engineered Cardiac Patch From Human Induced Pluripotent Stem Cell-Derived Cardiomyocytes in a Rat Infarct Model. Stem Cells Transl Med. 2015; 4(11):1324–1332. [PubMed: 26371342]

Wendel JS, Ye L, Zhang P, et al. Functional consequences of a tissue-engineered myocardial patch for cardiac repair in a rat infarct model. Tissue Eng Part A. 2014; 20(7–8):1325–1335. [PubMed: 24295499]

Williams AR, Trachtenberg B, Velazquez DL, et al. Intramyocardial stem cell injection in patients with ischemic cardiomyopathy: functional recovery and reverse remodeling. Circulation Research. 2011; 108(7):792–796. [PubMed: 21415390]

Yu J, Vodyanik MA, Smuga-Otto K, et al. Induced pluripotent stem cell lines derived from human somatic cells. Science. 2007; 318(5858):1917–1920. [PubMed: 18029452]

Zhang D, Shadrin IY, Lam J, et al. Tissue-engineered cardiac patch for advanced functional maturation of human ESC-derived cardiomyocytes. Biomaterials. 2013; 34(23):5813–5820. [PubMed: 23642535]

Zhang J, Wilson GF, Soerens AG, et al. Functional cardiomyocytes derived from human induced pluripotent stem cells. Circulation Research. 2009; 104(4):e30–41. [PubMed: 19213953]

Zhao YY, Sawyer DR, Baliga RR, et al. Neuregulins promote survival and growth of cardiac myocytes. Persistence of ErbB2 and ErbB4 expression in neonatal and adult ventricular myocytes. J Biol Chem. 1998; 273(17):10261–10269. [PubMed: 9553078]

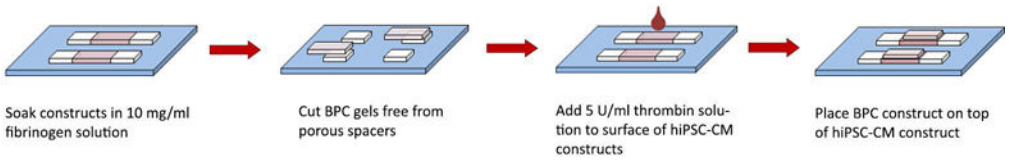

Figure 1.
Bi-layer patch formation schematic.

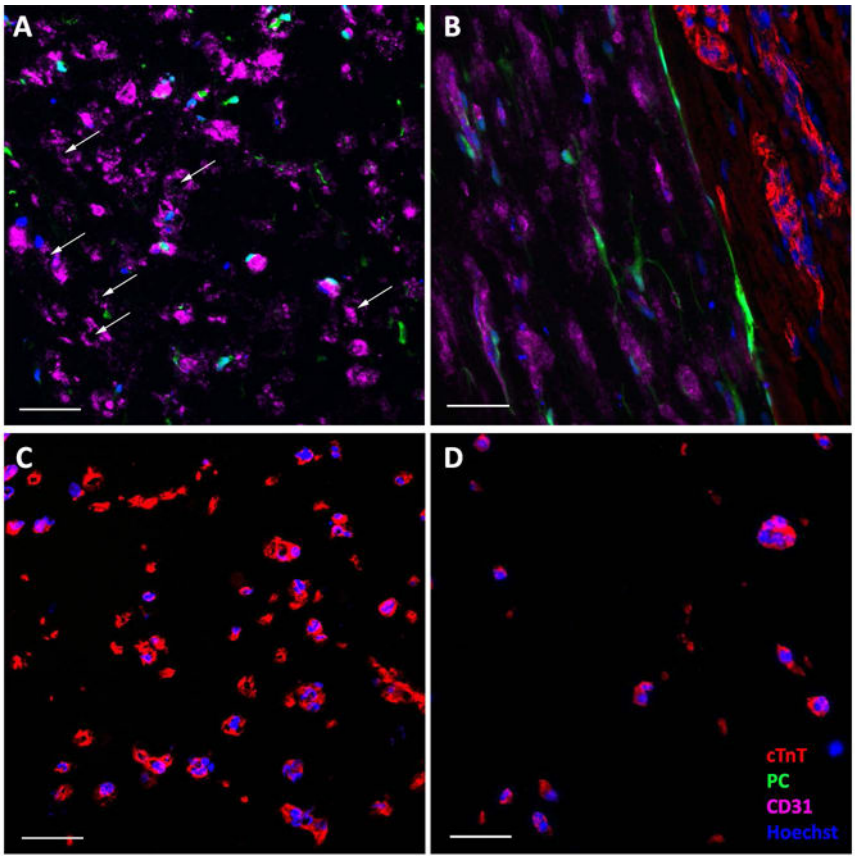

Figure 2.

Immunofluorescence characterization of patches before implantation. **A)** Cross-section of BPC layer of bi-layer patch. White arrows indicating microvessel lumens. **B)** Longitudinal section of bi-layer patch showing interface between the two layers and the alignment of both CMs (cTnT) and microvessels (CD31). **C)** Cross-sectional view of CM layer of bi-layer patch compared to time-matched **D)** cross-sectional view of CM-only patch. Abbreviations: cTnT, cardiac troponin-T; PC, pericytes. Color of labels is consistent in all panels. Scale bars = 50 μm.

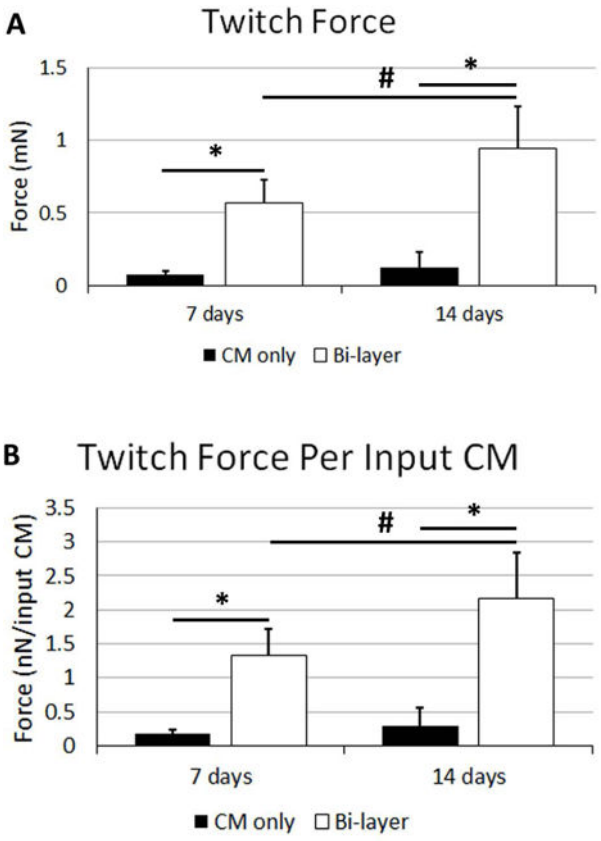

Figure 3.

Twitch force characterization of patches before implantation. Twitch force **A)** and twitch force normalized to the number of CMs seeded into the gels during gel formation **B)**. Significance is indicated by horizontal bars between groups, $p<0.05$.

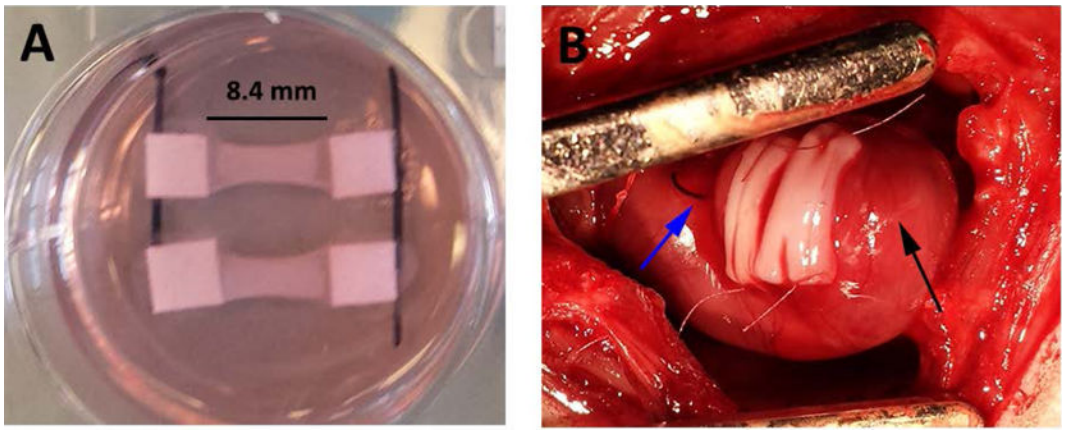

Figure 4.

Bi-layer patches at implantation. **A)** Patches prior to removing from spacers after two weeks of culture. **B)** Two patches sutured onto the left ventricular epicardial surface after myocardial infarction. Blue arrow indicates ligation suture, black arrow indicates apex of heart.

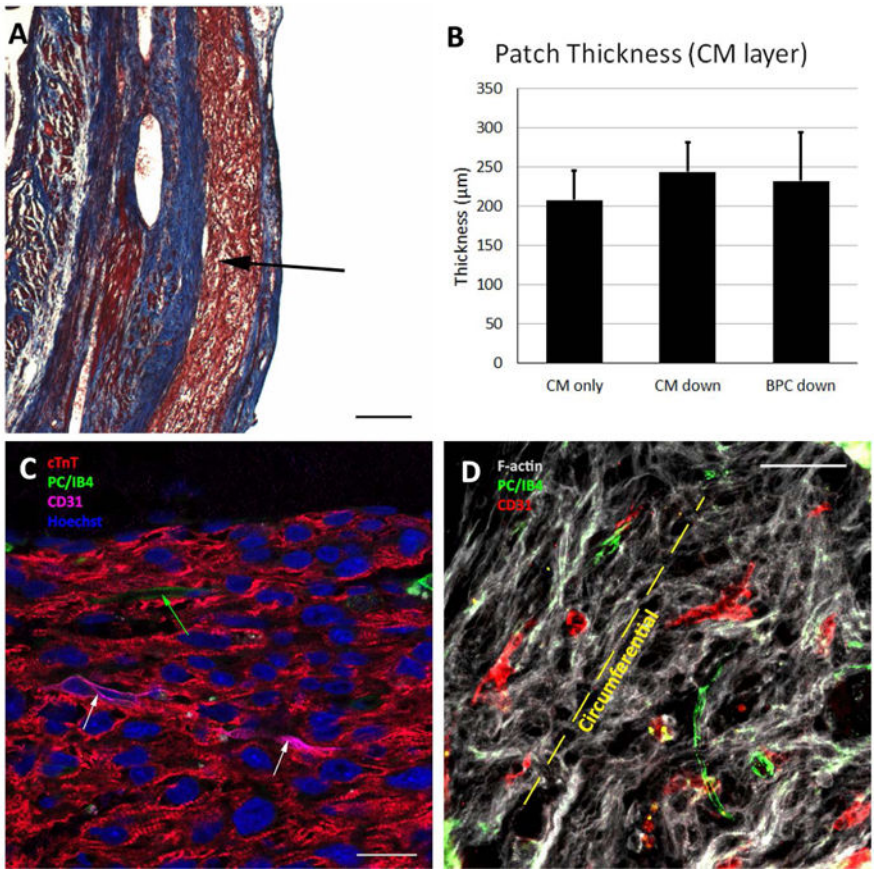

Figure 5.

Patch engraftment four weeks after implantation. **A)** Masson's trichrome image showing patch on the epicardium (arrow). Scale bar = 200 μm. **B)** Patch thickness for each of the three implant groups, where "CM down" and "BPC down" refers to the orientation of the implanted bi-layer patches. **C)** High magnification image of patch showing dense CM layer and sarcomeric banding. White arrows indicate human microvessels and green arrow indicates rat microvessel that have sprouted into the CM patch. Scale bar = 20 μm **D)** F-actin stain indicating alignment of CMs in the circumferential direction. Rat and human microvessels generally co-align with the CMs. Scale bar = 50 μm. Abbreviations: cTnT, cardiac troponin-T; PC, pericytes; IB4, fluorescein conjugated griffonia simplicifolia I, isolectin B4.

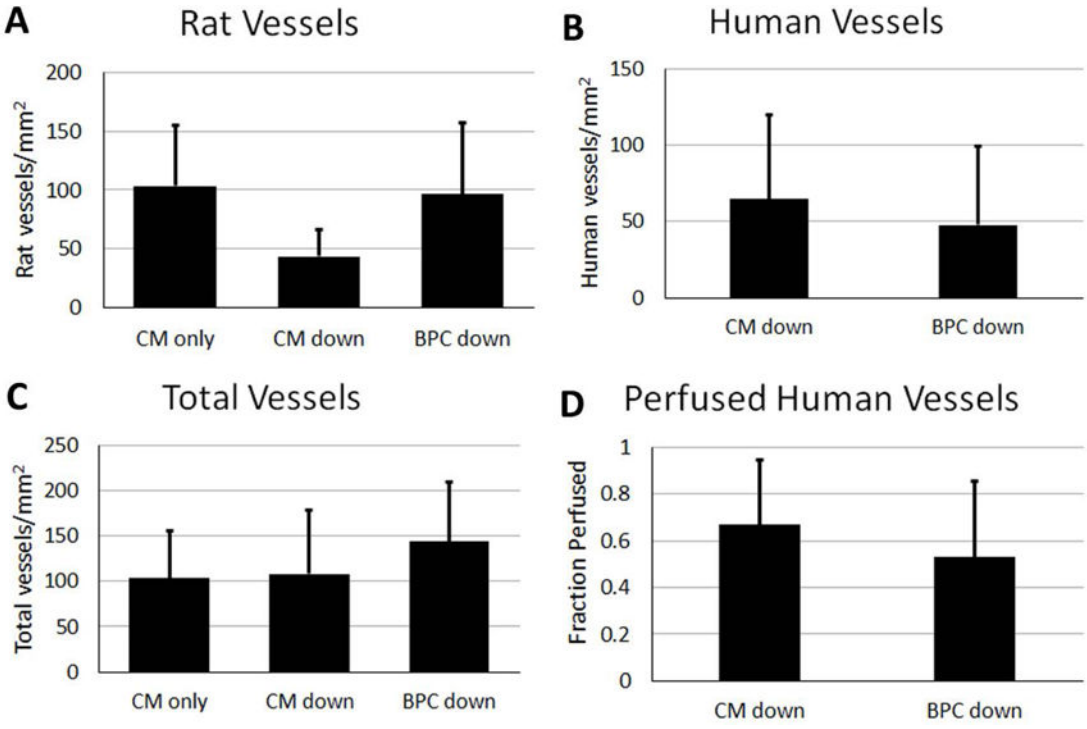

Figure 6.

Quantification of **A)** rat, **B)** human, and **C)** total vessels that sprouted into the CM layer of the bi-layer patch or CM-only patch. **D)** The fraction of human vessels that were perfused at time of explant based on co-localization of CD31 and human perfusion label.

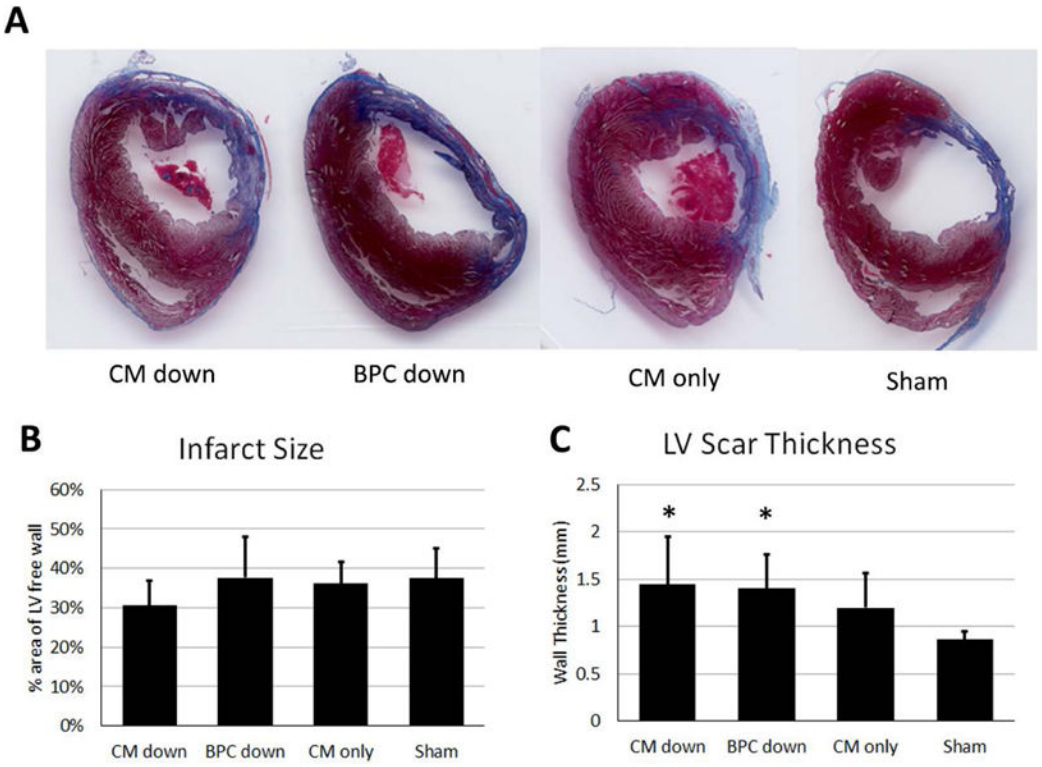

Figure 7.

Characterization of scar four weeks after infarction based on Masson's trichrome images. **A)** Representative images of the LV scar from the four groups. **B)** Scar size in terms of the percent area of the LV free wall it occupies. **C)** LV wall scar thickness. * indicate significantly difference than sham, $p<0.05$.